Int. J. Adv. Appl. Math. and Mech. 5(4) (2018) 10 – 20 (ISSN: 2347-2529)

Journal homepage: www.ijaamm.com

IJAAMM

International Journal of Advances in Applied Mathematics and Mechanics

Homoclinic Bifurcation in a parametrically driven nonlinearly damped Duffing-vander Pol oscillator

Research Article

M. V. Sethu Meenakshi[a], S. Athisayanathan[a], V. Chinnathambi[b,*], S. Rajasekar[c]

[a] *Department of Mathematics, St. Xavier's College, Palayamkottai-627 002, Tamilnadu, India*

[b] *Department of Physics, Sadakathullah Appa College, Tirunelveli-627 011, Tamilnadu, India*

[b] *School of Physics, Bharathidasan University, Tiruchirapalli 620 024, Tamilnadu, India*

(a, b Affiliated to Manonmaniam Sundaranar University, Abishekapatti-627 012, Tirunelveli, Tamilnadu, India)

Received 31 May 2018; accepted (in revised version) 26 August 2018

Abstract: The occurrence of homoclinic bifurcation in nonlinearly damped Duffing-vander Pol (DVP) oscillator with parametric and external excitations is studied both analytically and numerically. Using Melnikov method, an analytical threshold condition for the prediction of onset of horseshoe chaos is obtained. Melinkov threshold curves are drawn in different external parameters space. The threshold curves separating the chaotic and non-chaotic regions are obtained. The effect of parametric and external excitations with $\omega = \Omega$ and $\omega \neq \Omega$ are analysed on the horseshoe dynamics. For small amplitude of the external excitations,when the damping exponent (p) increased from small value, the onset of horseshoe chaos is decreased. But the result is opposite for the case of large amplitude of the external excitation. Analytical predictions are demonstrated through numerical simulation.

MSC: 37D45 • 34C37 • 34D10 • 34A08 • 37J20 • 37C29

Keywords: Duffing-vander Pol oscillator • Nonlinear damping • Parametric excitation • Homoclinic bifurcation • Melnikov method • Chaos

1. Introduction

For the past 20 years, there was a significant interest in studying parametrically driven systems [1–8]. The interest is due to the fact that parametrically excited dynamical systems describe various problems in engineering and physics. By external periodic and parametric excitations of a nonlinear dynamical systems give rise to complicated and unexpected behaviours of the solutions. The introduction of horseshoe into the dynamics, ie., transverse intersections of stable and unstable manifolds coming from hyperbolic fixed point of the associated Poincaré map are the source of such complicated behaviours.

In recent years, many research workers have paid attention to study the solutions of nonlinear differential equations by using various perturbation methods. Among these are the homotopy perturbation method [9–11], Melnikov perturbation method [12–15] and the variational iteration method [15–17]. Melnikov's analysis is a powerful analytical tool to provide an approximate criterion for the occurrence of hetero/homoclinic chaos in a wide class of dynamical systems. Its also an effective approach to detect chaotic dynamics and to analyse near homoclinic motion with deterministic or random pertubation. The method was applied by Jing et al. [18] to study the complex dynamics in

* Corresponding author.

E-mail address(es): veerchinnathambi@gmail.com (V. Chinnathambi), rajasekar@cnld.bdu.ac.in (S. Rajasekar).

pendulum equation with parametric and external excitations and by Siewe Siewe et al. [19, 20] to examine the occurrence of chaos in a parametrically driven extended Rayleigh oscillator and Φ^6-vander Pol oscillator with three-well potential. Wu et al. [21] and Schwalger et al. [22] attempted to suppress or generate chaos in $L\ddot{U}$ and Duffing systems using parametric perturbation. The effect of symmetry-breaking on the parametrically excited pendulum including bias term is investigated by Zhou et al. [23]]. Recently, Zhou et al. [24] investigated both analytically and numerically the chaotic motions of the DVP oscillator with external and parametric excitations and Miwadinou et al. [26] studied the effect of nonlinear dissipation on the basin boundaries of a driven two-well or catastropic single-well modified Rayleigh-Duffing oscillator.

In this paper, we investigate analytically and numerically the effect of parametric perturbation in nonlinearly damped DVP oscillator equation

$$\ddot{x} + \gamma\dot{x}(1-x^2)\,|\,\dot{x}\,|^{p-1} - \alpha^2 x + \beta x^3(1+\eta\cos\,\Omega t) = f\cos\omega t, \tag{1}$$

where γ is a damping parameter, p is a damping exponent, $\alpha > 0, \beta > 0$ are real parameters, η is the amplitude and Ω is the frequency of the parametric perturbation and f is the amplitude of the external periodic forcing and ω is the corresponding frequency. The nonlinear damping term is taken to be proportional to the power of the velocity, in the form $\gamma\dot{x}\,|\,\dot{x}\,|^{p-1}$. A similar nonlinear damping term was used previously by many researchers [27–31]. The motivation for our interest in this system is that it has wide range of applications in physics and biology. When $p = 1$ and $\eta = 0$, Eq. (1) serves as a basic model for self-excited oscillations in various disciplines [23–26]. Our objective here is to explore the occurrence of horseshoe chaos using both analytical and numerical techniques. In our present analysis we use the Melnikov method to study the influence of parametric perturbation on horseshoe dynamics.

In Eq.(1), the nonlinear damping is defined by the exponent p

$$dpt(\dot{x}) = \gamma\dot{x}\,|\,\dot{x}\,|^{p-1}\,. \tag{2}$$

In Fig. 1(a) we have plotted the above function (Eq. (2)) versus velocity ($v = \dot{x}$) for few values of p. From this figure, we note that $p < 0$ ($p = 0.1$) representing an important case which can be associated with a dry friction phenomenon [32, 33].

When $\gamma = 0, \eta = 0$ and $f = 0$, Eq. (1) corresponds to the following undamped and unexcited system

$$\ddot{x} - \alpha^2 x + \beta x^3 = 0. \tag{3}$$

The potential function of the unexcited system (Eq. (3)) is as follows

$$V(x) = -\frac{1}{2}\alpha^2 x^2 + \frac{1}{4}\beta x^4, \tag{4}$$

and then the Hamiltonian function associated to Eq. (4) is

$$H(x,y) = \frac{1}{2}y^2 - \frac{1}{2}\alpha^2 x^2 + \frac{1}{4}\beta x^4. \tag{5}$$

By analyzing the unperturbed system, we can observe that there are three different equilibria, one saddle fixed point $(x^*, y^*) = (0,0)$ and two center type fixed points $(x^*, y^*) = (\pm\alpha/\sqrt{\beta}, 0)$. There exist homoclinic orbits which connects the saddle to itself are given by

$$W^{\pm}(x_h(\tau), y_h(\tau)) = \left(\pm\alpha\sqrt{\frac{2}{\beta}}\,\mathrm{sech}\tau, \mp\alpha^2\sqrt{\frac{2}{\beta}}\,\mathrm{sech}\alpha\tau\,\tanh\alpha\tau\right), \quad \tau = t - t_0. \tag{6}$$

Stable manifolds ($W_s^{\pm}$) and unstable manifolds ($W_u^{\pm}$) of homoclinic orbits are indicated in Fig. 1(b). Periodic orbits are nested within and outside the homoclinic orbits.

The paper is organized as follows. In section II, we obtained the conditions of existence of the horseshoe chaos under parametric perturbation using Melinkov technique. Then the effect of parametric perturbation on horseshoe dynamics is analyzed in section III. The analytical prediction is demonstrated through numerical simulations. We end in section IV with conclusions.

2. Melnikov Analysis For the Parametric Perturbation

We now suppose that the unperturbed system discussed in the previous section is perturbed by a combination of parametric force $\eta\cos\Omega t$, periodic force $f\cos\omega t$ and dissipative term $(1-x^2)\dot{x}\,|\,\dot{x}\,|^{p-1}$. In this section, we will investigate analytically the condition for the onset of horseshoe chaos by applying Melnikov method to Eq. (1).

We consider the DVP equation with periodic parametric perturbation with the nonlinearly damped term,

$$\dot{x} = y \tag{7a}$$

$$\dot{y} = \alpha^2 x - \beta x^3 + \epsilon\left[-\beta x^3\eta\cos\Omega t - \gamma\,(1-x^2)\,y\,|y|^{p-1} + f\cos\omega t\right] \tag{7b}$$

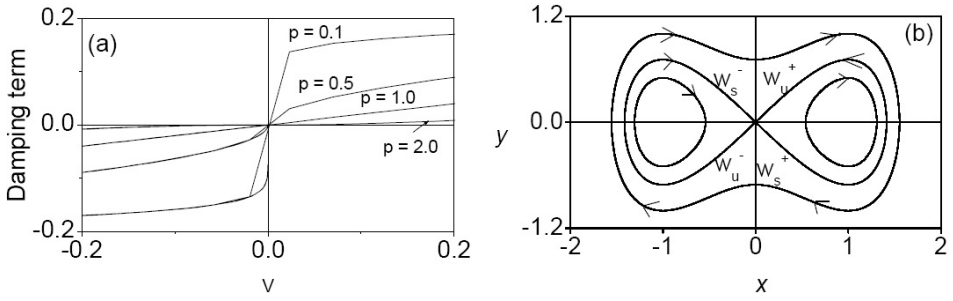

Fig. 1. (a) The function $dpt(\dot{x})$ versus $\dot{x}$ for few values of p. (b) Phase portrait of unperturbed system (Eq. (3)). The stable $(W_s^{\pm})$ and $(W_u^{\pm})$ parts of homoclinic orbits connecting saddle to itself are indicated. The analytical expression for the homoclinic orbits is given by Eq. (6)

where ϵ is a small parameter. Because the Melnikov method is based on the perturbation theory, we have introduced a small parameter ϵ in the equation of motion. Recently, Sethu Meenakshi et al. [34, 35] studied the effect of narrow-band frequency and amplitude modulated signals in nonlinearly damped DVP oscillator.

Now we compute the Melnikov function of the system (Eq.(7)) along the homoclinic orbit ((6)) as follows. For Eq.(7), Melnikov function is worked out to be

$$\begin{aligned} M(t_0) = -\gamma \int_{-\infty}^{\infty} (1-x_h^2)|y_h|^{p+1}\, d\tau + f\int_{-\infty}^{\infty} y_h \cos\omega(\tau+t_0)d\tau \\ -\beta\eta\int_{-\infty}^{\infty} y_h\, x_h^3 \cos\Omega(\tau+t_0)d\tau \\ = I_1 \quad + \quad I_2 \quad + \quad I_3 \end{aligned} \tag{8a}$$

where,

$$I_1 = -\gamma \int_{-\infty}^{\infty} (1-x_h^2)|y_h|^{p+1}\, d\tau \tag{8b}$$

$$I_2 = f\int_{-\infty}^{\infty} y_h \cos\omega(\tau+t_0)d\tau \tag{8c}$$

$$I_3 = -\beta\eta\int_{-\infty}^{\infty} y_h\, x_h^3 \cos\Omega(\tau+t_0)d\tau \tag{8d}$$

2.1. Calculation of I_1 :

From Eq. (8b), we have

$$\begin{aligned} I_1 = -\gamma\int_{-\infty}^{\infty} |y_h|^{p+1} d\tau + \gamma\int_{-\infty}^{\infty} |y_h|^{p+1}\, x_h^2 d\tau \\ = \quad I_{11} \quad + \quad I_{12} \end{aligned} \tag{9}$$

Using the explicit form of (x_h, y_h) given by Eq.(6) and by the application of some algebraic techniques, the integrals I_{11} and I_{12} are worked out to be

$$I_{11} = -\gamma(\alpha^2)^{p+\frac{1}{2}} \left[\frac{2}{\beta}\right]^{(p+1)/2} B\left[\frac{p+2}{2}, \frac{p+1}{2}\right] \tag{10a}$$

and

$$I_{12} = \gamma(\alpha^2)^{p+3/2} \left[\frac{2}{\beta}\right]^{(p+3)/2} B\left[\frac{p+2}{2}, \frac{p+3}{2}\right] \tag{10b}$$

Therefore

$$I_1 = -\gamma(\alpha^2)^{p+\frac{1}{2}} \left[\frac{2}{\beta}\right]^{(p+1)/2} B\left[\frac{p+2}{2}, \frac{p+1}{2}\right] + \gamma(\alpha^2)^{p+3/2} \left[\frac{2}{\beta}\right]^{(p+3)/2} B\left[\frac{p+2}{2}, \frac{p+3}{2}\right] \tag{10c}$$

where $B(m,n)$ is the Euler Beta function defined as $B(m,n) = \dfrac{\Gamma(m)\Gamma(n)}{\Gamma(m+n)}$, where $\Gamma(m)$ denotes the Euler gamma function, which is defined as $\Gamma(x) = \int_0^{\infty} t^{x-1}e^{-t}dt, \quad x>0.$

2.2. Calculation of I_2

From Eq. (8c) we have

$$\begin{aligned} I_2 &= f\int_{-\infty}^{\infty} y_h[\cos\omega\tau\cos\omega t_0 - \sin\omega\tau\ \sin\omega\ t_0]\,d\tau \\ &= f\ \cos\omega t_0\int_{-\infty}^{\infty} y_h\cos\omega\tau\,d\tau - f\sin\omega t_0\int_{-\infty}^{\infty} y_h\sin\omega\tau\,d\tau \\ &= \qquad I_{21} \qquad + \qquad I_{22} \end{aligned} \tag{11}$$

After the evaluation of the integral I_{21}, the integral value of $I_{21} = 0$ and the value of integral I_{22} is worked out to be

$$\begin{aligned} I_{22} &= \pm f\alpha^2\sqrt{\frac{2}{\beta}}\sin\omega t_0\int_{-\infty}^{\infty}\operatorname{sech}\alpha\tau\tanh\alpha\tau\ \sin\omega\tau\ d\tau \\ &= \pm\sqrt{\frac{2}{\beta}}f\pi\omega\operatorname{sech}\left[\frac{\pi\omega}{2\alpha}\right]\sin\omega t_0 \end{aligned}$$

therefore, the integral value of I_2 is

$$I_2 = \pm\sqrt{\frac{2}{\beta}}f\pi\omega\operatorname{sech}\left[\frac{\pi\omega}{2\alpha}\right]\sin\omega t_0 \tag{12}$$

2.3. Calculation of I_3 :

From Eq. (8d), we have,

$$\begin{aligned} I_3 &= -\beta\eta\int_{-\infty}^{\infty} y_h x_h^3\,[\cos\Omega\tau\ \cos\Omega t_0 - \sin\Omega\tau\ \sin\Omega t_0]\,d\tau \\ &= -\beta\eta\cos\Omega t_0\int_{-\infty}^{\infty} y_h x_h^3\cos\Omega\tau\,d\tau + \beta\eta\sin\Omega t_0\int_{-\infty}^{\infty} y_h x_h^3\sin\Omega\tau\,d\tau \\ &= \qquad I_{31} \qquad + \qquad I_{32} \end{aligned} \tag{13}$$

The integral value of I_{31} is zero. The value of integral I_{32} is worked out to be,

$$I_{32} = \beta\eta\sin\Omega_1 t_0\int_{-\infty}^{\infty} y_h x_h^3\sin\Omega\tau\ d\tau \tag{14}$$

$$= \mp\eta\ \frac{\pi}{6\beta}\ \Omega^2\ (4\alpha^2+\Omega^2)\ \operatorname{cosech}\left[\frac{\pi\Omega}{2\alpha}\right]\sin\Omega t_0 \tag{15}$$

Therefore,

$$I_3 = \mp\eta\ \frac{\pi}{6\beta}\ \Omega^2\ (4\alpha^2+\Omega^2)\ \operatorname{cosech}\left[\frac{\pi\Omega}{2\alpha}\right]\ \sin\Omega t_0. \tag{16}$$

Therefore the Eq. (8) becomes,

$$M(t_0) = A + B \pm fC\sin\omega t_0 \mp D\eta\sin\Omega t_0 \tag{17a}$$

where,

$$A = -\gamma(\alpha^2)^{p+\frac{1}{2}}\left[\frac{2}{\beta}\right]^{(p+1)/2} B\left[\frac{p+2}{2},\frac{p+1}{2}\right] \tag{17b}$$

$$B = \gamma(\alpha^2)^{p+3/2}\left[\frac{2}{\beta}\right]^{(p+3)/2} B\left[\frac{p+2}{2},\frac{p+3}{2}\right] \tag{17c}$$

$$C = \sqrt{\frac{2}{\beta}}\pi\omega\operatorname{sech}\left[\frac{\pi\omega}{2\alpha}\right] \tag{17d}$$

$$D = \frac{\pi}{6\beta}\ \Omega^2\ (4\alpha^2+\Omega^2)\ \operatorname{cosech}\left[\frac{\pi\Omega}{2\alpha}\right]. \tag{17e}$$

$M(t_0)$ is proportional to the distance between the stable manifolds (W_s) and unstable manifold (W_u) of a saddle. When the stable and unstable manifolds are separated then the sign of $M(t_0)$ always remain same. $M(t_0)$ oscillates when W_s and W_u intersects transversely (horseshoe dynamics). A zero of $M(t_0)$ corresponds to tangential intersection. The occurrence of transverse intersections implies that the Poincaré map of the system has the so-called *horseshoe chaos*.

3. Effect of Parametric Perturbation on Homoclinic Bifurcation

In this section we study the effect of parametric perturbation on homoclinic bifurcation. For $\eta \neq 0$ and $\omega = \Omega$, the necessary condition for $M(t_0)$ to change sign is

$$\eta^{\pm} \leq \eta_M = \frac{6\beta(-(A+B) \pm Cf)}{\pi\,\Omega^2(4\alpha^2+\Omega^2)} \sinh\left(\frac{\pi\,\Omega}{2\alpha}\right) \tag{18a}$$

or

$$\eta^{\pm} \geq \eta_M = \frac{6\beta((A+B) \pm Cf)}{\pi\,\Omega^2(4\alpha^2+\Omega^2)} \sinh\left(\frac{\pi\,\Omega}{2\alpha}\right) \tag{18b}$$

where the superscripts sign '+' and '-' correspond to the homoclinic orbits W^+ and W^- respectively. In the present work we analyse the parametric perturbation with small amplitude ($f = 0.2$) and large amplitude ($f = 1.0$) of the external periodic force. Figs. 2 and 3 show the threshold value of $\eta(\Omega)$ for $\Omega = \omega$. First taking $f = 0.2$, letting $\Omega = \omega$, for different values of p, we get the threshold curves separating the chaotic and non-chaotic regions as in Fig. 2. Next, letting $f = 1.0$, the threshold curves for different values of p are shown in Fig. 3. The values of the other parameters are $\alpha = 1.0, \beta = 5.0$ and $\gamma = 0.4$.

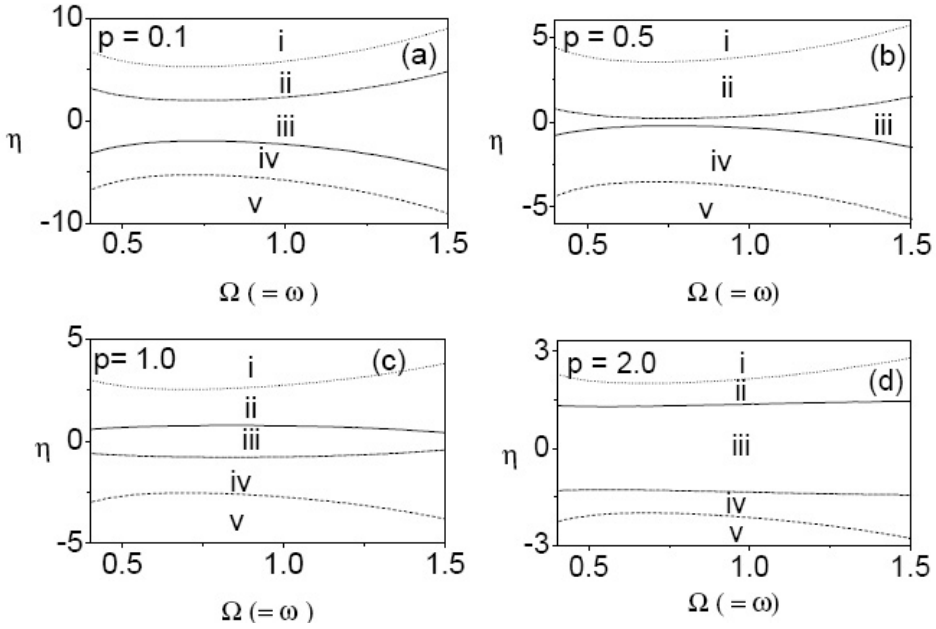

Fig. 2. Melnikov threshold curves for horseshoe chaos in the $(\eta, \Omega(=\omega))$ plane for the parametrically driven system (Eq. (7)) for four p values. The values of the other parameters in Eq.(7) are $\alpha = 1.0, \beta = 5.0, \gamma = 0.4$ and $f = 0.2$.

From Figs. 2 and 3, we can obtain the following conclusions

1. In the region (i), both $M^+(t_0)$ and $M^-(t_0)$ change sign. This implies that in this region transverse intersections of the orbits W_s^+ and W_u^+ and W_s^- and W_u^- occur.
2. In the region (ii), $M^+(t_0)$ alone changes sign and the sign of $M^-(t_0)$ remains same. This indicates that in the region the transverse intersection of the orbits W_s^+ and W_u^+ alone occur.
3. In the region (iii), $M^+(t_0)$ and $M^-(t_0)$ do not change sign. Consequently, in this region, no transverse intersection of stable and unstable orbits of saddle.
4. In the region (iv), transverse intersections of W_s^- and W_u^- alone take place since in this region only $M^-(t_0)$ changes sign.
5. In the region (v), both $M^+(t_0)$ and $M^-(t_0)$ change sign. This means that transverse intersections of stable and unstable parts of both W^+ and W^- occur.
6. . For $f = 0.2$ and $p = 2.0$, area of the periodic region is more than the other p valus such as $p = 0.1, 0.5$ and $p = 1.0$, which is clearly evident in Fig. 2. In Fig. 3, for $f = 1.0$, periodic motion (region III) increases as p increases.

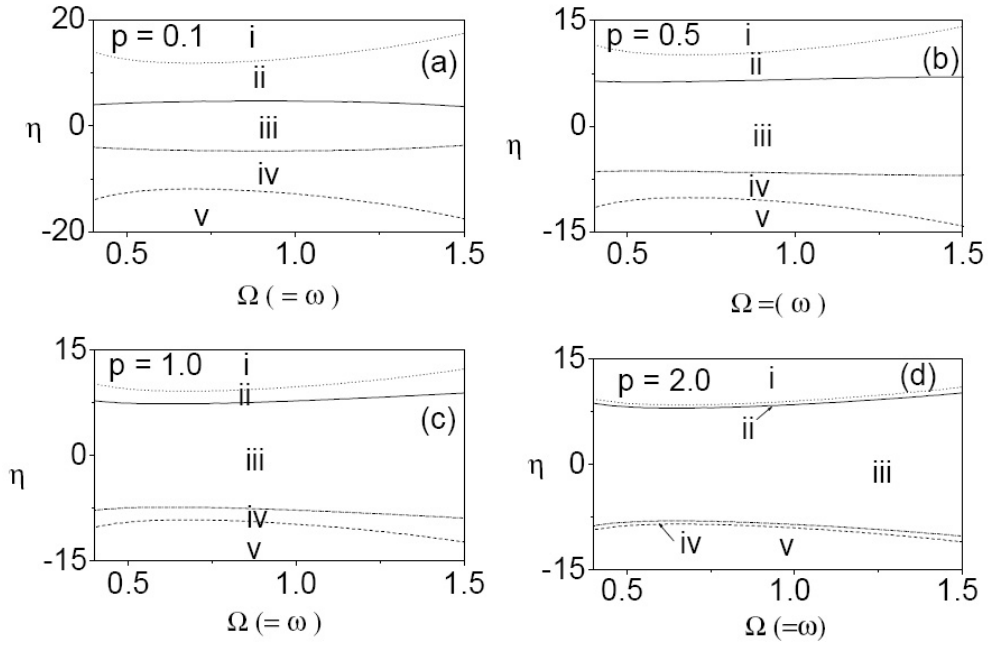

Fig. 3. Melnikov threshold curves for horseshoe chaos in the $(\eta, \Omega(=\omega))$ plane for the parametrically driven system (Eq. (7)) for four p values. The values of the other parameters in Eq. (7)) are $\alpha = 1.0, \beta = 5.0, \gamma = 0.4$ and $f = 1.0$.

7. The regions (i) and (v) (chaotic motions) almost the same in Figs.2 and 3 for all values of p. In Fig. 3, regions (ii) and (iv) decreases as p increases.

We have verified the above analytical predictions by numerically computing the stable and unstable manifolds of the saddle for $p = 0.5$. The other parameters values are fixed as $\alpha = 1.0, \beta = 5.0, \gamma = 0.4$ and $\omega = \Omega = 1.0$. Unstable manifolds are obtained by numerically integrating Eq. (1) by the fourth-order Runge-Kutta method in the forward time for a set of 900 initial conditions chosen around the perturbed saddle point. The stable manifolds are obtained by integrating the equation of motion in reverse time. As an example, Fig. 4 shows the part of stable and unstable orbits of saddle in the Poincare map for $p = 0.5, \omega = \Omega = 1.0, f = 0.2$ and four values of η chosen in the regions (i), (ii), (iii) and (iv) in Fig. 2.

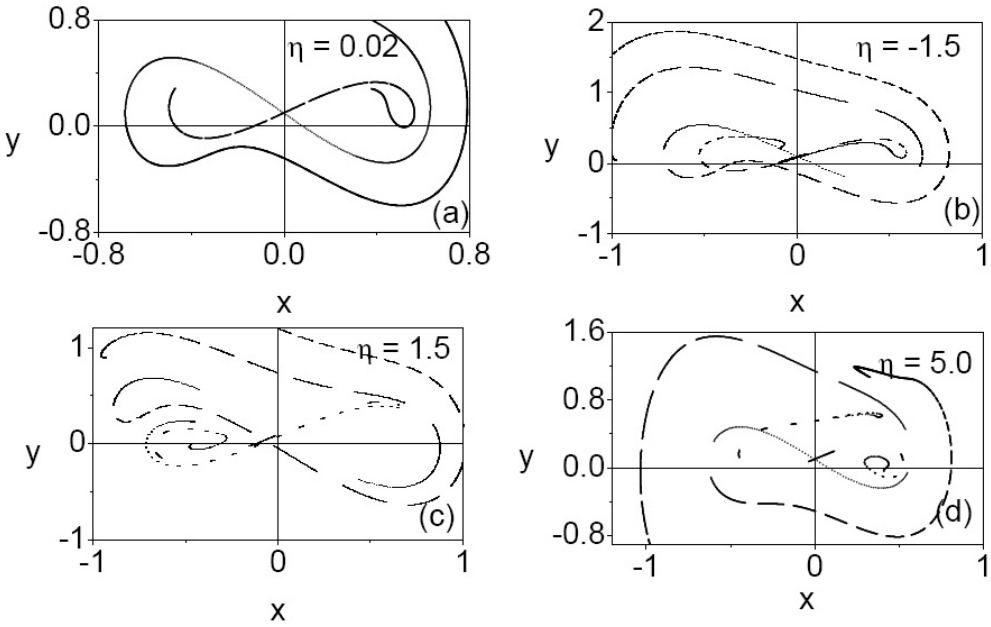

Fig. 4. Numerically computed stable and unstable manifolds of the saddle fixed point of the paramertically driven system (Eq. (7)) for four values of η chosen in the regions (i), (ii), (iii) and (iv) with $p = 0.5$. The values of the other parameters in Eq.(7) are $\alpha = 1.0, \beta = 5.0, \gamma = 0.4, f = 0.2$ and $\omega = \Omega = 1.0$.

Next we study the occurrence of homoclinic bifurcation numerically measuring the time τ_M elapsed between successive change in the sign of $M(t_0)$. τ_M can be determined from Eq. (17). We fix the parameters in Eq. (17) as $\alpha = 1.0, \beta = 5.0, \gamma = 0.4$ and $\omega = \Omega = 1.0$. Fig. 5 shows the variation of $1/\tau_M$ versus η for $f = 0.2$ and few values of p. The variation of $1/\tau_M$ versus η for $f = 1.0$ and few values of p is shown in Fig. 6. Continuous curve corresponds to positive sign while dashed curve corresponds to negative sign in Eq. (17). Horseshoe dynamics does not occur when $1/\tau_M$ is zero and it occurs in the region when $1/\tau_M > 0$.

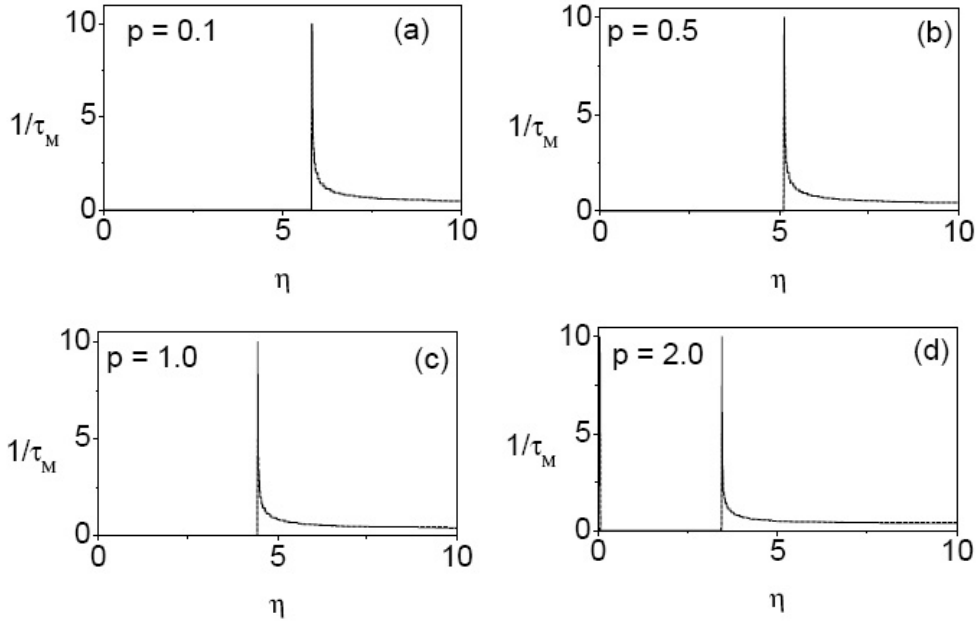

Fig. 5. Variation of $1/\tau_M^{\pm}$ versus η for $f = 0.2$ and four values of p. The values of the other parameters in Eq. (7) are $\alpha = 1.0, \beta = 5.0, \gamma = 0.4$, and $\Omega = \omega = 1.0$.

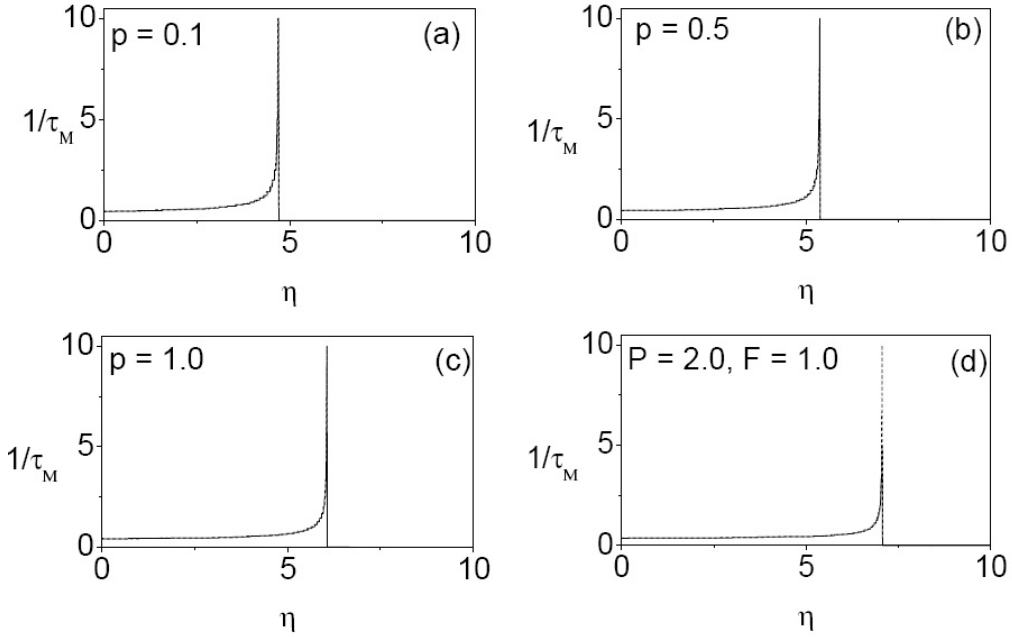

Fig. 6. Variation of $1/\tau_M^{\pm}$ versus η for $f = 1.0$ and four values of p. The values of the other parameters in Eq. (7) are $\alpha = 1.0, \beta = 5.0, \gamma = 0.4$, and $\Omega = \omega = 1.0$.

From Figs. 5 - 6, we obtain the following conclusions

1. in Fig. 5(a), for $f = 0.2$ and $p = 0.1$, both $1/\tau_M^{+}$ and $1/\tau_M^{-}$ are zero (that is $\tau^{\pm}$ are infinity) in the interval $0 < \eta <$

5.815. This implies that horseshoe chaos does not occur for $\eta < \eta_M^{\pm} = 5.815$. For $\eta > 5.815$, both $M^+(t_0)$ and $M^-(t_0)$ oscillate and hence $1/\tau_M^{\pm}$ are non-zero. For $\eta > \eta_M^{\pm}$ horseshoe chaos is possible. One clear observation from the Figs. 5(b), 5(c) and 5(d) is that, the threshold for horseshoe chaos η_M increases when the damping exponent (p) decreases The Melnikov threshold value (η_M) for $p = 0.1, 0.5, 1.0$ and 2.0 are $\eta_M^{\pm} = 5.815, 5.130, 4.441$ and 3.452.

2. In Fig. 6(a), for $f = 1.0$ and $p = 0.1$, $1/\tau_{M^+}$ and $1/\tau_{M^-}$ are non-zero for $\eta < \eta_M^{\pm} = 4.712$, that is horseshoe chaos is possible for $\eta < \eta_M^{\pm} = 4.712$. For $\eta > \eta_M^{\pm} = 4.712$, horseshoe chaos does not occur. As p increases the threshold for horseshoe chaos (η_M) also increases which are clearly evident in Figs. 6(b), 6(c) and 6(d). The case is opposite for $f = 0.2$ (Fig. 5). The Melnikov threshold ($\eta_M^{\pm}$) values for horseshoe chaos for $p = 0.1, 0.5, 1.0$ and 2.0 are $\eta_M = 4.712, 5.390, 6.083$ and 7.074.

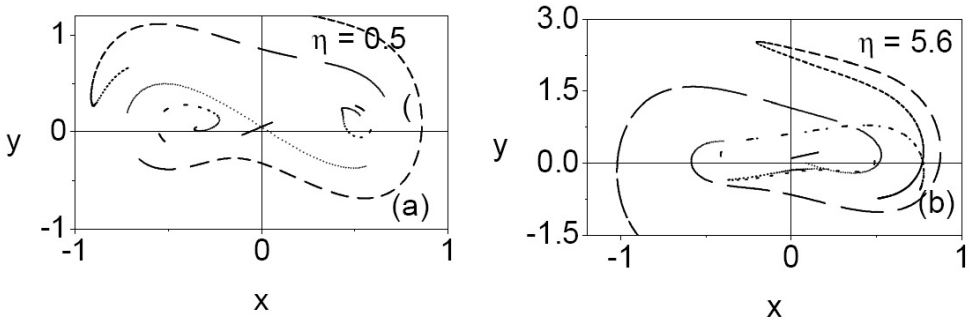

Fig. 7. Numerically computed stable and unstable manifolds of the saddle fixed point of the paramertically driven system (Eq. (7)) for two values of η with $p = 0.5$. The values of the other parameters in Eq. (7) are $\alpha = 1.0, \beta = 5.0, \gamma = 0.4$, $f = 0.2$ and $\omega = \Omega = 1.0$.

The above analytical results are verified numerically. Fig. 7 shows the part of stable and unstable orbits in the Poincaré map for two values of η chosen around the critical values of $\eta_M^{\pm}$ for $f = 0.2$ (Fig. 5) and $f = 1.0$ (Fig. 6). For $\eta = 0.5$, $f = 0.2$ and $p = 0.5$, there is no transverse intersection of stable and unstable orbits of the saddle as in Fig. 7(a) and for $\eta = 5.6$, transverse intersections of stable and unstable orbits in $x < 0$ and $x > 0$ are clearly seen in Fig. 7(b).

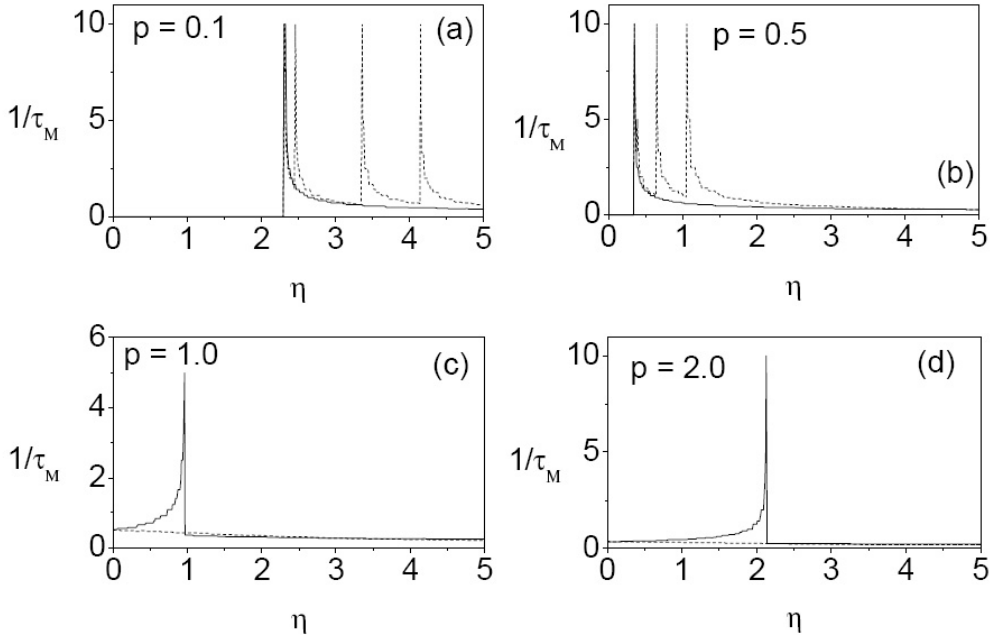

Fig. 8. Variation of $1/\tau_M^{\pm}$ versus η for $f = 0.2$ and four values of p. The values of the other parameters in Eq.(7) are $\alpha = 1.0, \beta = 5.0, \gamma = 0.4$, $\Omega = (\sqrt{5}-1)/2$ and $\omega = 1.0$.

Finally we consider the effect of parametric perturbation for the case of $\Omega \neq \omega$. In Fig. 8, we have plotted $1/\tau_M^{\pm}$ as a function of η for $\omega = 1.0, \Omega = \frac{\sqrt{5}-1}{2}$ and four values of p. The other parameters values are fixed at $\alpha = 1.0, \beta = 5.0, f =$

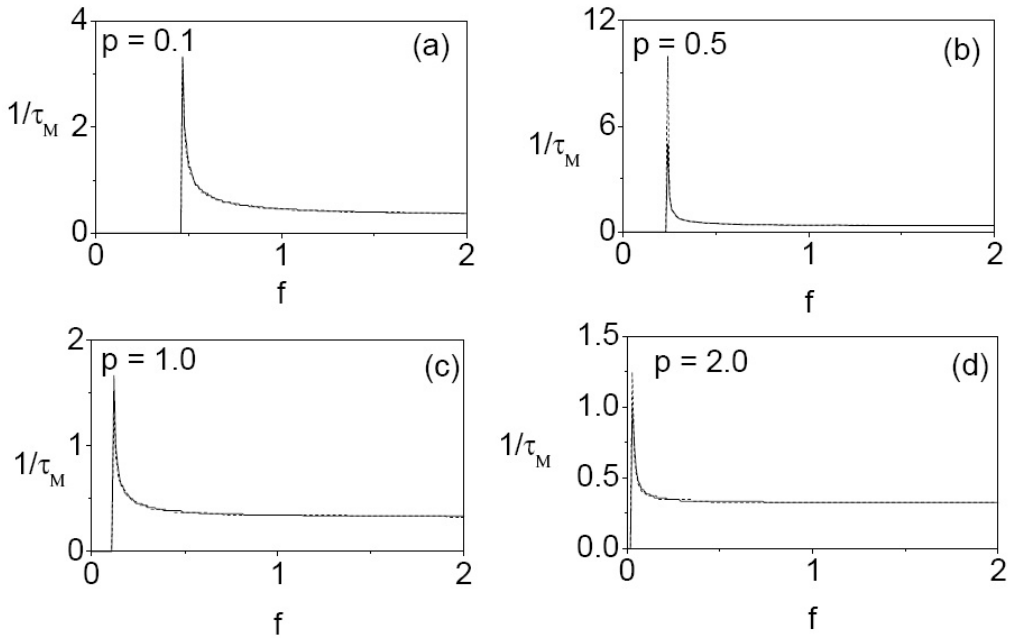

Fig. 9. Variation of $1/\tau_M^{\pm}$ versus f for $\eta = 0.02$ and four values of p. The values of the other parameters in Eq.(7) are $\alpha = 1.0, \beta = 5.0, \gamma = 0.4$, $\Omega = (\sqrt{5}-1)/2$ and $\omega = 1.0$.

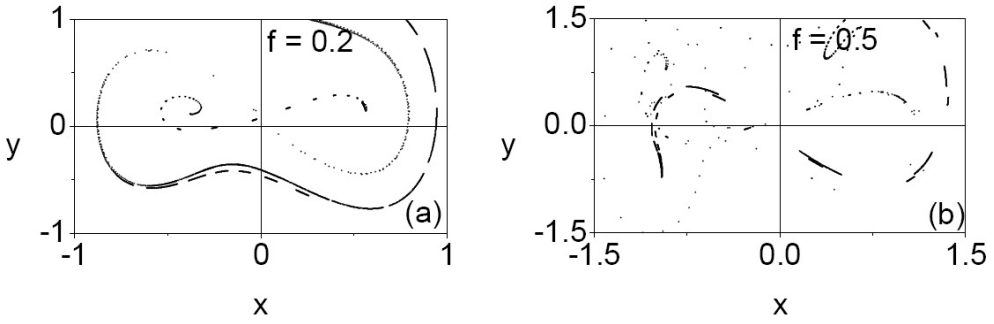

Fig. 10. Numerically computed stable and unstable manifolds of the saddle fixed point of the paramertically driven system (Eq. (7)) for two values of f with $p = 0.5$. The values of the other parameters in Eq. (7) are $\alpha = 1.0, \beta = 5.0, \gamma = 0.4, \eta = 0.02$, $\Omega = (\sqrt{5}-1)/2$ and $\omega = 1.0$.

0.2 and $\gamma = 0.4$. In Fig. 8 where the value of f is fixed at 0.2, $1/\eta_M^{\pm}$ are zero for $0 < \eta < 2.310$ for $p = 0.1$ (Fig. 8(a)) and $0 < \eta < 0.342$ for $p = 0.5$ (Fig. 8(b)) and hence no horseshoe chaos occurs in this interval of η. For $p \geq 1$ only horseshoe chaos is possible, which is clearly shown in Figs. 8 (c) and (d). Fig. 9 shows the plot of $1/\tau_M^{\pm}$ versus f for $\eta = 0.002, \omega = 1, \Omega = \frac{\sqrt{5}-1}{2}$ and four values of p. As p increases the region of horseshoe chaos increases, which is clearly evident in Fig. 9. The critical values of the threshold (f_M) for horseshoe chaos for $p = 0.1, 0.5, 1.0$ and 2.0 are 0.462, 0.233, 0.112 and 0.021. The above analytical results are verified numerically. Figure 10 shows the part of stable and unstable orbits in the Poincaré map for two values of f chosen around the critical values of $f_M^{\pm}$ for $\eta = 0.02$ (Fig. 9). For $f = 0.2$ and $p = 0.5$, there is no transverse intersection of stable and unstable orbits of the saddle as in Fig. 10(a) and $f = 0.5$, transverse intersection of stable and unstable orbits are clearly seen in Fig. 10(b).

4. Conclusion

Using the Melnikov and numerical methods, the occurrence of horseshoe chaos for the nonlinearly damped DVP oscillator with external and parametric excitations are investigated in this paper. Applying Melnikov analytical method, we obtained the threshold for the onset of horseshoe chaos, that is transverse intersections of stable and unstable branches of homoclinic orbits. In the present work, we have analysed the effect of parametric and external

excitations with the frequencies $\omega = \Omega$ and $\omega \neq \Omega$. Threshold curves are drawn in various parameters space. The Melnikov threshold curves separating the chaotic and non-chaotic regions are obtained.

For $\omega = \Omega$, when the amplitude (f) of the external excitation is fixed at small value ie., $f = 0.2$, as p increases, horseshoe chaos occurs at $\eta > \eta_M^{\pm}$ but for the higher values of f (ie.,$f > 1$) horseshoe chaos occurs at $\eta < \eta_M^{\pm}$ (Figs.5 and 6). For $\omega \neq \Omega$ and $f = 0.2$, no horseshoe chaos occurs for $p < 1$ but for $p \geq 1$ only horseshoe chaos is possible (Fig. 8). For $\omega \neq \Omega$ and $\eta = 0.02$ the threshold for horseshoe ($f_M^{\pm}$) decreases as p increases (Fig. 9). It is important to study the effect of parametric excitation in nonlinearly damped DVP oscillator with other excitations such as sinusoidal and nonsinusoidal, amplitude and frequency modulated forces. This will be investigated in future.

References

[1] B. Bruhn: Homoclinic bifurcation in simple parametrically driven systems, Ann.Physik Leipzig, 16(5), (1989) 367-375.

[2] J. Heagy, W.L. Ditto: Dynamics of a two-frequency parametrically driven Duffing oscillator, Journal of Nonlinear Science, 1, (1991) 422-455.

[3] S. Rajasekar: Controlling of chaos by weak periodic pertubation in Duffing-vander Pol oscillator, Pramana Journal of Physics, 4, (1993) 295-309.

[4] A.M. Abou-Rayan, A.H. Nayfeh, D.T. Mook: Nonlinear responce of a parametrically excited buckled beam, Nonlinear Dynamics, 4, (1993) 449-525.

[5] R. Chacon, A. Martinez Garcia-Hoz: Bifurcations and chaos in a parametrically damped two-well Duffing oscillator subjected to symmetric periodic pulses, Physical Review E, 59(6), (1999) 6553-6568.

[6] M.A.F. Sanjuan: Subharmonic bifurcations in a pendulum parametrically excited by a non-harmonic perturbation, Chaos, Solitons & Fractals, 9(6), (1998) 995-1003.

[7] M. Belhaq, M. Houssni: Quasi-periodic oscillations, chaos and supperssion of chaos in a nonlinear oscillator driven by parametric and external excitations, Nonlinear Dynamics, 18, (1999) 1-24.

[8] Y.S Kivshar, F. R*ö*delsperger, E. Benner: Suppression of chaos by nonresonant parametric perturbations, Physical Review E, 49(1), (1994) 319-324.

[9] S. Gupta, D. Kumar, J. Singh: Application of He's homotopy perturbation method for solving nonlinear equation with variable coefficients, Int. J. Adv. Appl. Math. and Mech., 1(2), (2013) 65-79.

[10] H. Kamil Jassim; Homotopy perturbation algorithm using Laplace transform for Newell Whitehead -Segel equation, Int. J. Adv. Appl. Math. and Mech., 2(6), (2015) 8-12.

[11] H.A. Hoshyar , D.D. Ganji, M. Abbasi: Analytical solution for porous fin with temperature-dependent heat generation via Homotopy perturbation method, Int. J. Adv. Appl. Math. and Mech., 2(3), (2015) 15-22.

[12] J. Guckenheimer, P. Holmes: The nonlinear oscillations, dynamical systems and bifurcations of vector fields, Springer, New York, (1983).

[13] S. Wiggins: Introduction to applied nonlinear dynamical systems and chaos, Springer, New York, (1990).

[14] E. Ott: Chaos in dynamical systems, Cambridge University Press, New York, (1993).

[15] M. Lakshmanan, S. Rajasekar: Nonlinear dynamics: Integrability, Chaos and Patterns, Springer, Berlin, (2003).

[16] J.H. He, X.H. Wu: Variational iteration method: new development and applications, Computers & Mathematics with Applications, 54, (2007) 881-894.

[17] J.H. He, G.C. Wu, F. Austin :The variational iteration method which should be followed, Nonlinear Science Letters A, 1, (2009) 1-30.

[18] Z. Jing, J. Yang: Complex dynamics in pendulum equation with parametric and external excitations, Int. J. of Bifur. & Chaos, 16(10), (2006) 3053-3078.

[19] M. Siewe Siewe, H. Cao, M.A.F. Sanjuan: On the occurrence of chaos in parametrically driven extended Rayleigh oscillator with three-well potential, Chaos, Solitons & Fractals, 41, (2009) 772-782.

[20] M. Siewe Siewe, F.M. Moukam kakmeni, C. Tchawana, P. Woafo: Bifurcations and chaos in the triple-well ϕ^6-vander Pol oscillator driven by external and parametric excitations, Physica A, 357, (2005) 383-396.

[21] X. Wu, J. Lu, H.H.C. Iu, S.C. Wong: Suppressions and generation of chaos for a three-dimensional autonomous system using parametric perturbations, Chaos, Solitions & Fractals, 31, (2007) 811-819.

[22] T. Schwalger, A. Dzhanoev, A. Loskutov: May chaos always be suppressed by parametric perturbations?, Chaos, 16, (2006) 023109(7PP).

[23] P. Zhou, H. Cao: The Effect of symmetry breaking on the parametrically excited pendulum, Chaos, Solitons & Fractals, 38, (2008) 590-597.

[24] L. Zhou, F. Chen: Chaotic motions of the Duffing-vander Pol oscillator with external and parametric excitations, Hindawi Publishing Corporation, Shock and Vibration, Vol.2014, Article ID 131637, 5pages.

[25] C.H. Miwsdinou, A.V. Monwanou, J.B. Chabi Orou: Effect of nonlinear dissipation on the basin boundaries of a drivrn two-well or catastropic single-well modified Rayleigh-Duffing oscillator, arXiv:1310.0958V3 [nlin,CD] 20

Dec., 2012.
[26] J.L. Trube, J. Rams, M.A.F. Sanjuan: Analytical estimates of the effect of nonlinear damping in some nonlinear oscillators, Int. J. of Bifur. & Chaos, 10(9), (2000) 2257-2267.
[27] M.A.F. Sanjuan: The Effect of nonlinear damping on the universal escape oscillator, Int. J. of Bifur. & Chaos, 9(4), (1999) 735-744.
[28] G. Litak, M. Borowiec, A. Syta: Vibration of generalized double-well oscillators, arXiv:nlin/0610052V1, [nlin.CD] 20 Oct. 2006.
[29] M. Borowiec, G. Litak, A. Syta: Vibration of Duffing oscillator: Effect of fractional damping, Shock & Vibration, 14, (2007) 29-36.
[30] J.L. Truba, J.P. Baltanas, M.A.F. Sanjuan: Nonlinearly damped oscillations, Recent Res. Devel. Sound & Vibration, 1, (2002) 29-61
[31] J.P. Baltanas, J.L. Truba, M.A.F. Sanjuan: Energy dissipation in a nonlinearity damped Duffing oscillator, Physica D, 159, (2001) 22-34.
[32] C.A. Brockley, P.L. Ko: Quasi-harmonic friction-induced vibration: ASME Journal of Lubrication Technology, 92, (1970) 550-556.
[33] R.A. Ibrahim: Friction-induced vibration, chatter, squeal and chaos. Part I: Mechanics of contact and friction, Appl. Mech. Rev., 47, (1994) 209-226.
[34] M.V. Sethu Mennakshi, S. Athisayanathan, V. Chinnathambi, S. Rajasekar: Effect of narrow band frequency modulated signal on horseshoe chaos in nonlinearly damped Duffing-vander Pol oscillator, Annual Review of Chaos Theory, Bifurcations and Dynamical Systems, 7, (2017) 41-55.
[35] M.V. Sethu Mennakshi, S. Athisayanathan, V. Chinnathambi, S. Rajasekar: Analytical estimates of the ampplitude modulated signal in nonlinearly damped Duffing-vander Pol oscillator, Chinese Journal of Physics, 55, (2017) 2208-2217.